CHIN. PHYS. LETT. Vol. 38, No. 4 (2021) 042101

# Constraining Isovector Nuclear Interactions with Giant Dipole Resonance and Neutron Skin in $^{208}$Pb from a Bayesian Approach

Jun Xu(徐骏)[1,2*]

[1] *The Interdisciplinary Research Center, Shanghai Advanced Research Institute, Chinese Academy of Sciences, Shanghai 201210, China*

[2] *Shanghai Institute of Applied Physics, Chinese Academy of Sciences, Shanghai 201800, China*

(Received 17 December 2020; accepted 25 January 2021; published online 6 April 2021)

The remaining uncertainties in relation to isovector nuclear interactions call for reliable experimental measurements of isovector probes in finite nuclei. Based on the Bayesian analysis, although neutron-skin thickness data or isovector giant dipole resonance data in $^{208}$Pb can constrain only one isovector interaction parameter, correlations among other parameters can also be built. Using combined data for both the neutron-skin thickness and the isovector giant dipole resonance helps to significantly constrain all isovector interaction parameters; as such, it serves as a useful methodology for future research.

DOI: 10.1088/0256-307X/38/4/042101

Extracting the properties of nuclear interactions from observables in finite nuclei is an effective approach to understanding strong interactions with fewer uncertainties. Thanks to pioneering studies by nuclear physicists, isoscalar nuclear interactions are so far better constrained; however, larger uncertainties still exist, mainly in relation to isovector nuclear interactions, impeding a more accurate understanding of the properties of radioactive nuclei, dynamics in nuclear reactions induced by neutron-rich nuclei, and many other interesting astrophysical phenomena, such as gravitational waves emerging from neutron-star mergers. On the one hand, isovector nuclear interactions can be manifested in the isospin-dependent part of the nuclear matter equation of state, i.e., the nuclear symmetry energy $E_{\rm sym}$,[1–4] which is generally characterized by the value $E_{\rm sym}^0$ at the saturation density $\rho_0 = 0.16\,{\rm fm}^{-3}$, as well as its slope parameter $L = 3\rho_0(dE_{\rm sym}/d\rho)_{\rho_0}$ around the saturation density. In recent years, constraints of $E_{\rm sym}(\rho_0) = 31.7 \pm 3.2\,{\rm MeV}$ and $L = 58.7 \pm 28.1\,{\rm MeV}$ have been obtained from surveying 53 analyses carried out by 2016, using various terrestrial nuclear laboratory data and astrophysical observations;[5,6] however, more accurate constraints are still called for. On the other hand, isovector nuclear interactions also determine the properties of single-nucleon potentials in neutron-rich medium. As a result of momentum-dependent single-nucleon potential, nucleons move with an effective mass, $m^*$, rather than a free mass, $m$, in nuclear matter, similarly to the case of electron dynamics near the gap between energy bands in semiconductors. Different neutron and proton effective masses affect not only isospin-dependent nucleon dynamics in heavy-ion collisions, but also the properties of neutron-rich nuclei.[7] Since both nuclear symmetry energy $E_{\rm sym}$ and neutron-proton effective mass splitting $m^*_{\rm n-p} = m^*_{\rm n} - m^*_{\rm p}$ originate from isovector nuclear interactions, it is not surprising that they are related to each other through the Hugenholtz–van Hove theorem.[5,8]

This study serves as an attempt to constrain isovector nuclear interactions manifested by nuclear symmetry energy and neutron-proton effective mass splitting via the properties of $^{208}$Pb, a heavy spherical nucleus free from ambiguities in terms of clustering, deformation, etc. We focus primarily on the isovector giant dipole resonance (IVGDR) and the neutron-skin thickness in $^{208}$Pb. The isovector giant dipole resonance can be considered as a collective excitation mode, with neutrons and protons moving relatively to each other in a nucleus like a harmonic oscillator, where the symmetry energy acts as a restoring force,[9–18] while the nucleon effective mass, which is an analogue of the oscillator mass, may also affect the dynamics;[19,20] as such, the de-excitation spectrum, measured experimentally, can function as a means of probing both properties. The neutron-skin thickness, defined as the difference between neutron and proton rms radii in a nucleus, is primarily due to a stronger pressure for neutrons than that for protons, and is one of the most robust and sensitive probes of the symmetry energy slope parameter.[21–33] Although each observable is not expected to pin down both symmetry energy and neutron-proton effective mass splitting, we will show that using both observables in the same

Supported by the National Natural Science Foundation of China (Grant No. 11922514).

*Corresponding author. Email: xujun@zjlab.org.cn; xujun@sari.ac.cn

© 2021 Chinese Physical Society and IOP Publishing Ltd

$^{208}$Pb nucleus helps to constrain significantly isovector nuclear interactions.

For the theoretical calculation of isovector giant dipole resonance and neutron-skin thickness, we use the Skyrme–Hartree–Fock (SHF) model, originating from the following effective interaction between two nucleons at $\boldsymbol{r}_1$ and $\boldsymbol{r}_2$:

$$\begin{aligned} v(\boldsymbol{r}_1,\boldsymbol{r}_2) =& t_0(1+x_0P_\sigma)\delta(\boldsymbol{r}) + \frac{1}{2}t_1(1+x_1P_\sigma)[\boldsymbol{k}'^2\delta(\boldsymbol{r}) \\ &+ \delta(\boldsymbol{r})\boldsymbol{k}^2] + t_2(1+x_2P_\sigma)\boldsymbol{k}'\cdot\delta(\boldsymbol{r})\boldsymbol{k} \\ &+ \frac{1}{6}t_3(1+x_3P_\sigma)\rho^\alpha(\boldsymbol{R})\delta(\boldsymbol{r}) + iW_0(\boldsymbol{\sigma}_1+\boldsymbol{\sigma}_2) \\ &\cdot[\boldsymbol{k}'\times\delta(\boldsymbol{r})\boldsymbol{k}]. \end{aligned} \tag{1}$$

Here, $\boldsymbol{r} = \boldsymbol{r}_1 - \boldsymbol{r}_2$ and $\boldsymbol{R} = (\boldsymbol{r}_1 + \boldsymbol{r}_2)/2$, respectively, represent the relative and the central coordinate, $\boldsymbol{k} = (\nabla_1 - \nabla_2)/2i$ is the relative momentum operator, with $\boldsymbol{k}'$ as its complex conjugate acting on the left, and $P_\sigma = (1 + \boldsymbol{\sigma}_1\cdot\boldsymbol{\sigma}_2)/2$ is the spin exchange operator, with $\boldsymbol{\sigma}_{1(2)}$ being the Pauli matrices. The spin-orbit coupling constant is fixed at $W_0 = 133.3\,\text{MeV}\cdot\text{fm}^5$. Instead of the usual fitting process, the other 9 SHF parameters, $t_0$, $t_1$, $t_2$, $t_3$, $x_0$, $x_1$, $x_2$, $x_3$, and $\alpha$, can be inversely solved from 9 macroscopic quantities characterizing the saturation properties of nuclear matter,[34] including the isoscalar and isovector nucleon effective mass $m^*_{\rm s}$ and $m^*_{\rm v}$ at the Fermi momentum in normal nuclear matter, and the symmetry energy $E^0_{\rm sym}$ and its slope parameter $L$ at the saturation density. The isoscalar nucleon effective mass, $m^*_{\rm s}$, is the nucleon effective mass in isospin symmetric nuclear matter, while the isovector nucleon effective mass, $m^*_{\rm v}$, is the proton (neutron) effective mass in pure neutron (proton) matter. Up to the linear order of the isospin asymmetry, $\delta$, neutron-proton effective mass splitting is related to $m^*_{\rm s}$ and $m^*_{\rm v}$ via the relation

$$m^*_{\rm n} - m^*_{\rm p} \approx \frac{2m^*_{\rm s}}{m^*_{\rm v}}(m^*_{\rm s} - m^*_{\rm v})\delta. \tag{2}$$

Determining the SHF parameters from expressions of macroscopic quantities[34] provides the possibility of changing the value of only one of them, while keeping the same values for others; in this way, one can investigate the effect on observables from only one particular macroscopic quantity. In this study, we fix $m^*_{\rm s} = 0.83m$ in order to approximately reproduce the excitation energy of the isoscalar giant quadruple resonance, independent of other macroscopic quantities, and change only one individual quantity, e.g., $E^0_{\rm sym}$, $L$, or $m^*_{\rm v}$, at a time, while keeping the values of other macroscopic quantities at their empirical values given in Table I of Ref. [34].

Based on the Hartree–Fock method, the effective interaction in Eq. (1) leads to the standard SHF energy-density functional,[35] with time-odd terms neglected in the calculation of spin-saturated spherical nuclei. With the single-nucleon Hamiltonian obtained via the variational principle from the energy-density functional,[36] the nucleon wave functions can be calculated based on the Schrödinger equation, giving us the nucleon density distributions. The Reinhard SHF code[37] is used to calculate the nucleon density distribution and the neutron-skin thickness $\Delta r_{\rm np}$ in $^{208}$Pb via the above standard procedure.

With the nucleon wave functions obtained from the Hartree–Fock method, the random-phase approximation (RPA) method can be used to calculate the strength function of a particular nucleus resonance,

$$S(E) = \sum_\nu |\langle\nu||\hat{F}_J||\tilde{0}\rangle|^2\delta(E - E_\nu), \tag{3}$$

where the square of the reduced matrix element, $|\langle\nu||\hat{F}_J||\tilde{0}\rangle|$, represents the transition probability from the ground state, $|\tilde{0}\rangle$, to the excited state, $|\nu\rangle$, with $\hat{F}_J$ being the operator of the nucleus excitation. For IVGDR, the operator can be expressed as

$$\hat{F}_{1\rm M} = \frac{N}{A}\sum_{i=1}^{Z} r_iY_{1\rm M}(\hat{r}_i) - \frac{Z}{A}\sum_{i=1}^{N} r_iY_{1\rm M}(\hat{r}_i), \tag{4}$$

where $N$, $Z$, and $A$ represent the neutron, proton, and nucleon numbers in a nucleus, respectively, $r_i$ is the coordinate of the $i$th nucleon with respect to the center-of-mass of the nucleus, and $Y_{1\rm M}(\hat{r}_i)$ denotes the spherical Bessel functions, with the magnetic quantum number $M$ degenerate in spherical nuclei. The two observables characterizing the strength function of IVGDR, i.e., the centroid energy, $E_{-1}$, and the electric polarizability, $\alpha_D$, can be obtained from the moments of the strength function

$$m_k = \int_0^\infty dE E^k S(E) \tag{5}$$

through the relations

$$E_{-1} = \sqrt{m_1/m_{-1}},\ \alpha_D = \frac{8\pi e^2}{9}m_{-1}. \tag{6}$$

The open source code developed in Ref. [38] is used to calculate the $E_{-1}$ and $\alpha_D$ of the IVGDR in $^{208}$Pb, using the RPA method, based on the SHF model.

We have employed the Bayesian analysis method to obtain the probability distribution function (PDF) of the symmetry energy $E_{\rm sym}$, and the isovector nucleon effective mass $m^*_{\rm v}$ from the neutron-skin thickness $\Delta r_{\rm np}$, as well as the centroid energy $E_{-1}$ and the electric polarizability $\alpha_D$ in $^{208}$Pb. How the experimental data improves our knowledge of model parameters can be described by Bayes' theorem, formally written as

$$P(M|D) = \frac{P(D|M)P(M)}{\int P(D|M)P(M)dM}. \tag{7}$$

Here, $P(M|D)$ is the posterior PDF for the model $M$, given the experimental data $D$, which is seen to be normalized by the denominator of the right-hand side. $P(M)$ denotes the prior PDF of the model $M$ prior to being confronted with the experimental data, and we choose the prior PDFs of the model parameters $p_1 = L$, uniformly distributed within (0, 120) MeV, $p_2 = E^0_{\rm sym}$, uniformly distributed within (25, 35) MeV, and $p_3 = m^*_{\rm v}/m$, uniformly distributed within (0.5, 1). In this way, we investigate what information $\Delta r_{\rm np}$ and/or IVGDR alone can provide in terms of the model parameters, though the use of PDFs from previous studies may introduce additional information on the posterior PDFs of these parameters. Within these large prior distribution ranges of isovector interaction parameters, the binding energies and charge radii of $^{208}$Pb deviate by only a few percent at most,[34] demonstrating that we are exploring a reasonable parameter space. Here, $P(D|M)$ is the likelihood function, describing how well the theoretical model, $M$, predicts the experimental data, $D$, and it is defined as

$$P[D(d_{1,2,3})|M(p_{1,2,3})] = \Pi_i \frac{1}{\sqrt{2\pi}\sigma_i} \exp\Big[-\frac{(d_i^{\rm exp} - d_i^{\rm theo})^2}{2\sigma_i^2}\Big], \quad (8)$$

where $d_{1,2,3}$ represent the experimental data of $\Delta r_{\rm np}$, $E_{-1}$, and $\alpha_D$ in $^{208}$Pb, respectively, and $d_i^{\rm theo}$ and $d_i^{\rm exp}$ denote, respectively, the theoretical result and the mean value of the experimental result of the $i$th observable. In principle, $\sigma_i$, denoting the width of the likelihood function, represents both the experimental and theoretical error, while it is chosen as the $1\sigma$ error bar of the experimental measurement for the purposes of this study. For the IVGDR in $^{208}$Pb, the centroid energy $E_{-1} = 13.46$ MeV was accurately measured from photoneutron scatterings,[39] and the electric polarizability $\alpha_D = 19.6 \pm 0.6\,{\rm fm}^3$ was obtained from polarized proton inelastic scatterings,[40] with the quasi-deuteron excitation contribution subtracted.[15] An artificial error bar of 0.1 MeV is used for the well-determined $E_{-1}$ value of the IVGDR. For the neutron-skin thickness in $^{208}$Pb, the values of $\Delta r_{\rm np}$ are different, based on different measurements. For example, $\Delta r_{\rm np} = 0.211^{+0.054}_{-0.063}$ fm and $0.16 \pm 0.07$ fm were obtained from proton[41] and pion[42] scatterings, respectively, $\Delta r_{\rm np} = 0.18 \pm 0.04({\rm expt.}) \pm 0.05({\rm theor.})$ fm was obtained from the annihilation of antiprotons on the nuclear surface,[43,44] $\Delta r_{\rm np} = 0.15 \pm 0.03({\rm stat.})^{+0.01}_{-0.03}({\rm sys.})$ fm was obtained from coherent pion photoproductions,[45] and $\Delta r_{\rm np} = 0.33^{+0.16}_{-0.18}$ fm was measured from parity-violating electron scatterings.[46] In our study, we use the imagined experimental data of $\Delta r_{\rm np} = 0.15$ and 0.20 fm, each with imagined error bars of 0.02 and 0.06 fm, while awaiting new data from the lead ($^{208}$Pb) radius experiment at the Jeferson Laboratory, and the Mainz radius experiment at the Mainz energy recovery superconducting accelerator.[30] The calculation of the posterior PDFs is based on the Markov–Chain Monte Carlo approach, using the Metropolis–Hastings algorithm, and the samples are analyzed after convergence without the initial burn-in steps. The PDF of a single model parameter $p_i$ is given by

$$P(p_i|D) = \frac{\int P(D|M)P(M)\Pi_{j\neq i}dp_j}{\int P(D|M)P(M)\Pi_j dp_j}, \quad (9)$$

while the correlated PDF of the two model parameters, $p_i$ and $p_j$, is given by

$$P[(p_i,p_j)|D] = \frac{\int P(D|M)P(M)\Pi_{k\neq i,j}dp_k}{\int P(D|M)P(M)\Pi_k dp_k}. \quad (10)$$

In Fig. 1, we begin by showing the correlated posterior PDFs of isovector interaction parameters from imagined neutron-skin thickness data, or those from the IVGDR data for $^{208}$Pb, following integration of the third isovector interaction parameter. It is remarkable to see that $L$ and $E^0_{\rm sym}$ are anticorrelated with each other, based on the neutron-skin thickness data, while they are positively correlated based on the IVGDR data. For more discussions relating to this behavior, we refer the reader to the appendix of Ref. [47]. It is interesting to see that the PDFs of $L$ are mostly independent of $m^*_{\rm v}$, based on the neutron-skin thickness data, while those of $m^*_{\rm v}$ are mostly independent of $L$ and $E^0_{\rm sym}$ based on the IVGDR data, except for the cut-off due to the limited prior distribution ranges of $L$ and $E^0_{\rm sym}$, as can be understood from their correlation within the limited ranges in panel (i). The posterior PDFs of $m^*_{\rm v}/m$, $L$, and $E^0_{\rm sym}$ based on the imagined neutron-skin thickness data with different error bars, or those based on the IVGDR data in $^{208}$Pb, are displayed in Fig. 2. It is seen that neutron-skin thickness alone is unable to constrain $m^*_{\rm v}$ or $E^0_{\rm sym}$, and only constrains $L$ within $35^{+19}_{-26}$ and $74^{+17}_{-25}$ MeV at a 68% confidence level around its maximum *a posteriori* (MAP) values, for $\Delta r_{\rm np} = 0.15 \pm 0.02$ and $0.20 \pm 0.02$ fm, respectively. However, the PDFs of $L$ become broader if the error bar changes from 0.02 fm to 0.06 fm, demonstrating less constraining power in the latter case. On the other hand, the IVGDR data alone is unable to constrain $L$ or $E^0_{\rm sym}$ simultaneously, but constrains $m^*_{\rm v}/m$ within $0.79 \pm 0.04$ at a 68% confidence level around its MAP value, consistent with the results obtained in Ref. [48].

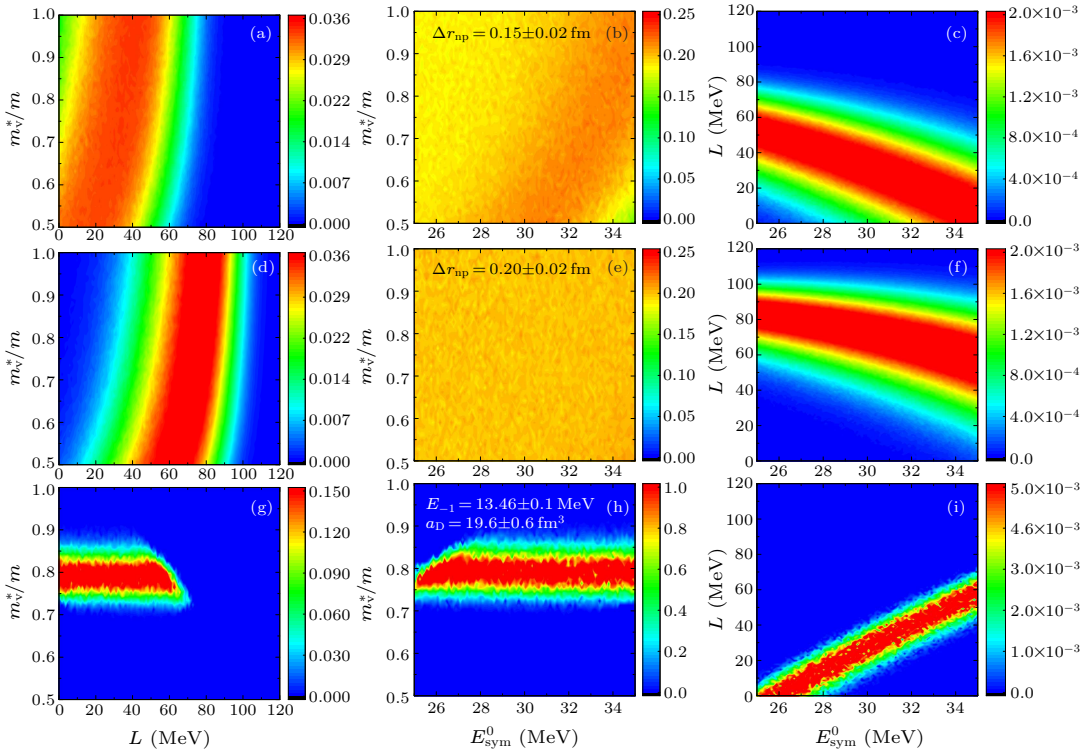


**Fig. 1.** Correlated posterior PDFs from the neutron-skin thickness data of $\Delta r_{\rm np} = 0.15 \pm 0.02$ fm (upper panels), $\Delta r_{\rm np} = 0.20 \pm 0.02$ fm (middle panels), or the IVGDR data (lowest panels) in $^{208}$Pb in the $L - m_{\rm v}^*/m$ plane (left), the $E_{\rm sym}^0 - m_{\rm v}^*/m$ plane (middle), and the $E_{\rm sym}^0 - L$ plane (right).

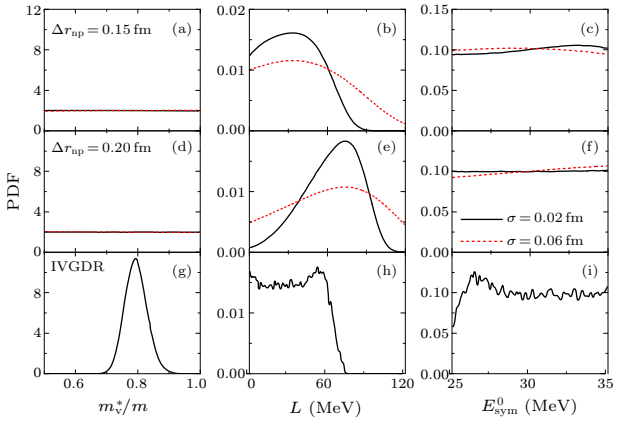


**Fig. 2.** Posterior PDFs from the neutron-skin thickness data for $\Delta r_{\rm np} = 0.15$ fm (upper panels) or $\Delta r_{\rm np} = 0.20$ fm (middle panels) with error bars 0.02 and 0.06 fm, and from the IVGDR data (lowest panels) in $^{208}$Pb for $m_{\rm v}^*/m$ (left), $L$ (middle), and $E_{\rm sym}^0$ (right).

Although neutron-skin thickness data and the IVGDR data, taken individually, can each pin down only one isovector interaction parameter, the data can lead to correlations between other parameters, based on the Bayesian approach. Combining both the neutron-skin thickness and the IVGDR data in $^{208}$Pb helps significantly to constrain all three isovector interaction parameters, $m_{\rm v}^*$, $L$, and $E_{\rm sym}^0$, as shown in Figs. 3 and 4. We note that incorporating the IVGDR data slightly reduces the MAP value of the $L$ PDF, from about 35 MeV to 31 MeV for $\Delta r_{\rm np} = 0.15 \pm 0.02$ fm, and from about 74 MeV to 55 MeV for $\Delta r_{\rm np} = 0.20 \pm 0.02$ fm, respectively. On the other hand, incorporating the neutron-skin thickness data has almost no effect on the PDF of $m_{\rm v}^*$. Since $L$ and $E_{\rm sym}^0$ are correlated, $E_{\rm sym}^0$ is also constrained around a MAP value of about 30 MeV based on $\Delta r_{\rm np} = 0.15 \pm 0.02$ fm and IVGDR data, but is greater than 35 MeV for $\Delta r_{\rm np} = 0.20 \pm 0.02$ fm and IVGDR data, if the range of $E_{\rm sym}^0$ is enlarged. Again, neutron-skin thickness data with a larger error bar of 0.06 fm do not change the PDF of $m_{\rm v}^*$, but lead to broader PDFs of both $L$ and $E_{\rm sym}^0$. This study calls for real data with respect to the neutron-skin thickness in $^{208}$Pb, taken from a more reliable experimental measurement.

To summarize, we have studied the constraints on the isovector interaction parameters, i.e., the symmetry energy at the saturation density $E_{\rm sym}^0$, the slope parameter of the symmetry energy $L$, and the isovector nucleon effective mass, $m_{\rm v}^*$, based on the imagined neutron-skin thickness data and the real isovector giant dipole resonance (IVGDR) data in $^{208}$Pb, via a Bayesian approach. Although the neutron-skin thickness data can only constrain $L$, and the IVGDR data can only constrain $m_{\rm v}^*$, they facilitate correlations between other parameters. Combining both the neutron-skin thickness data and the IVGDR data helps to constrain significantly all three isovector interaction parameters.

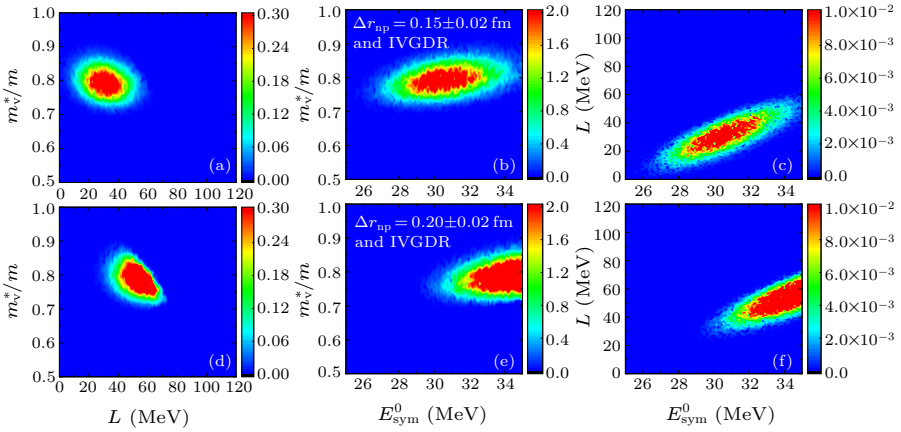


**Fig. 3.** Correlated posterior PDFs combining the neutron-skin thickness data [$\Delta r_{\rm np} = 0.15 \pm 0.02$ fm (upper panels) or $\Delta r_{\rm np} = 0.20 \pm 0.02$ fm (lower panels)] and the IVGDR data in $^{208}$Pb in the $L - m_{\rm v}^*/m$ plane (left), the $E_{\rm sym}^0 - m_{\rm v}^*/m$ plane (middle), and the $E_{\rm sym}^0 - L$ plane (right).

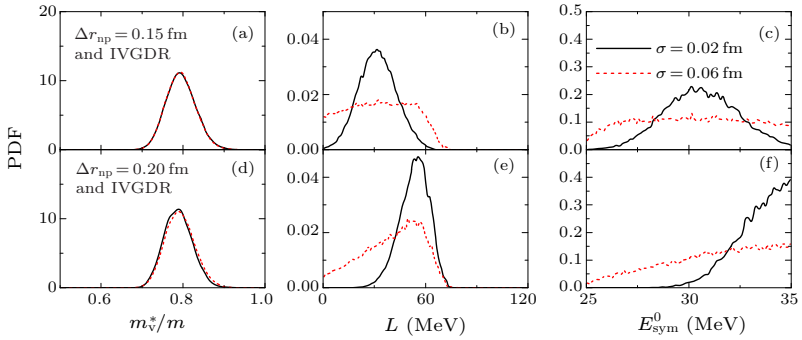


**Fig. 4.** Posterior PDFs based on combining the neutron-skin thickness data [$\Delta r_{\rm np} = 0.15$ fm (upper panels) or $\Delta r_{\rm np} = 0.20$ fm (lower panels) with error bars 0.02 and 0.06 fm], and the IVGDR data in $^{208}$Pb for $m_{\rm v}^*/m$ (left), $L$ (middle), and $E_{\rm sym}^0$ (right).

This study is based on the Skyrme–Hartree–Fock model, together with the random-phase approximation method. We note that the correlation between model parameters can be built with given experimental data, e.g., the neutron-skin thickness and IVGDR, while the Bayesian analysis serves as a useful tool with which to reveal that correlation. A slightly different correlation could be obtained from different theoretical models, e.g., the relativistic mean-field model. It would be very interesting to investigate the model-dependence of this type of study, and to use additional experimental data in order to offer a more robust constraint of model parameters by employing a Bayesian analysis.

The author thanks Bao-An Li and Wen-Jie Xie for helpful discussions.

## References

[1] Baran V, Colonna M, Greco V and Di Toro M 2005 *Phys. Rep.* **410** 335
[2] Steiner A W, Prakash M, Lattimer J M and Ellis P J 2005 *Phys. Rep.* **411** 325
[3] Lattimer J M and Prakash M 2007 *Phys. Rep.* **442** 109
[4] Li B A, Chen L W and Ko C M 2008 *Phys. Rep.* **464** 113
[5] Li B A and Han X 2013 *Phys. Lett. B* **727** 276
[6] Oertel M, Hempel M, Klähn T and Typel S 2017 *Rev. Mod. Phys.* **89** 015007
[7] Li B A, Cai B J, Chen L W and Xu J 2018 *Prog. Part. Nucl. Phys.* **99** 29
[8] Xu C, Li B A and Chen L W 2010 *Phys. Rev. C* **82** 054607
[9] Trippa L, Colò G and Vigezzi E 2008 *Phys. Rev. C* **77** 061304(R)
[10] Reinhard P G and Nazarewicz W 2010 *Phys. Rev. C* **81** 051303(R)
[11] Piekarewicz J, Agrawal B K, Colò G, Nazarewicz W, Paar N, Reinhard P G, Roca-Maza X and Vretenar D 2012 *Phys. Rev. C* **85** 041302(R)
[12] Vretenar D, Niu Y F, Paar N and Meng J 2012 *Phys. Rev. C* **85** 044317
[13] Roca-Maza X, Brenna M, Colò G, Centelles M, Vi N X, Agrawal B K, Paar N, Vretenar D and Piekarewicz J 2013 *Phys. Rev. C* **88** 024316
[14] Colò G, Garg U and Sagawa H 2014 *Eur. Phys. J. A* **50** 26
[15] Roca-Maza X, Vi N X, Centelles M, Agrawal B K, Colò G, Paar N, Piekarewicz J and Vretenar D 2015 *Phys. Rev. C* **92** 064304
[16] Zhang Z and Chen L W 2015 *Phys. Rev. C* **92** 031301(R)
[17] Zheng H, Burrello S, Colonna M and Baran V 2016 *Phys. Rev. C* **94** 014313
[18] Xu J and Qin W T 2020 *Phys. Rev. C* **102** 024306
[19] Zhang Z and Chen L W 2016 *Phys. Rev. C* **93** 034335
[20] Kong H Y, Xu J, Chen L W, Li B A and Ma Y G 2017 *Phys. Rev. C* **95** 034324
[21] Brown B A 2000 *Phys. Rev. Lett.* **85** 5296

[22] Typel S and Brown B A 2001 *Phys. Rev. C* **64** 027302
[23] Horowitz C J and Piekarewicz J 2001 *Phys. Rev. Lett.* **86** 5647
[24] Furnstahl R J 2002 *Nucl. Phys. A* **706** 85
[25] Todd-Rutel B G and Piekarewicz J 2005 *Phys. Rev. Lett.* **95** 122501
[26] Centelles M, Roca-Maza X, Viñas X and Warda M 2009 *Phys. Rev. Lett.* **102** 122502
[27] Zhang Z and Chen L W 2013 *Phys. Lett. B* **726** 234
[28] Agrawal B K, Malik T, De J N and Samaddar S K 2020 arXiv:2006.05758 [nucl-th]
[29] Behera D, Tripathy S K, Routray T R and Behera B 2020 *Phys. Scr.* **95** 105301
[30] Thiel M, Sfienti C, Piekarewicz J, Horowitz C J and Vanderhaeghen M 2019 *J. Phys. G* **46** 093003
[31] Burgio G F and Vidaña I 2020 *Universe* **6** 119
[32] Vi X, Centelles M, Roca-Maza X and Warda M 2014 *Eur. Phys. J. A* **50** 27
[33] Roca-Maza X and Paar N 2018 *Prog. Part. Nucl. Phys.* **101** 96
[34] Chen L W, Li B A, Ko C M and Xu J 2010 *Phys. Rev. C* **82** 024321
[35] Chabanat E, Bonche P, Haensel P, Meyer J and Schaeffer R 1997 *Nucl. Phys. A* **627** 710
[36] Vautherin D and Brink D M 1972 *Phys. Rev. C* **5** 626
[37] Reinhard P G 1991 *Computational Nuclear Physics 1: Nuclear Structure* ed Langanke K, Maruhn J A and Koonin S E (New York: Springer-Verlag) chap 2 p 209
[38] Colò G, Cao L, Van Gia N and Capelli L 2013 *Comput. Phys. Commun.* **184** 142
[39] Dietrich S S and Berman B L 1988 *At. Data Nucl. Data Tables* **38** 199
[40] Tamii A, Poltoratska I, vonNeumann-Cosel P *et al.* 2011 *Phys. Rev. Lett.* **107** 062502
[41] Zenihiro J, Sakaguchi H, Murakami T, Yosoi M, Yasuda Y, Terashima S, Iwao Y, Takeda H, Itoh M, Yoshida H P and Uchida M 2010 *Phys. Rev. C* **82** 044611
[42] Friedman E 2012 *Nucl. Phys. A* **896** 46
[43] Klos B *et al.* 2007 *Phys. Rev. C* **76** 014311
[44] Brown B A, Shen G, Hillhouse G C, Meng J and Trzcinska A 2007 *Phys. Rev. C* **76** 034305
[45] Tarbert C M *et al.* 2014 *Phys. Rev. Lett.* **112** 242502
[46] Abrahamyan S *et al.* 2012 *Phys. Rev. Lett.* **108** 112502
[47] Xu J, Xie W J and Li B A 2020 *Phys. Rev. C* **102** 044316
[48] Xu J, Zhou J, Zhang Z, Xie W J and Li B A 2020 *Phys. Lett. B* **810** 135820